



## ORIGINAL ARTICLE

# A surface architected metal–organic framework for targeting delivery: Suppresses cancer growth and metastasis



Wen Xie, Feiya Zhou, Xiang Li, Zhichen Liu, Manyu Zhang, Zhihui Zong, Lili Liang\*

Department of Chemistry, Bengbu Medical College, Donghai Avenue, Bengbu 233030, Anhui, PR China

Received 1 November 2021; accepted 26 December 2021

Available online 31 December 2021

## KEYWORDS

Nanocarriers;  
MOFs;  
Targeting;  
Metastasis;  
Apoptosis

**Abstract** Porous nanosized metal–organic frameworks (MOFs) are becoming possible candidates as drug-delivery nanocarriers for their versatile porous structures and large loadings of drugs. However, controlling synthesis of MOFs with uniform morphology, good biocompatibility and targeting drug delivery is still a challenge, which greatly limits their clinical applications. Herein, a multifunctional nano-sized drug-delivery material MIL-101(Fe)@FU@FA with a uniform particle size about 500 nm was successfully synthesized for targeting therapeutic purposes. The targeting reagent folic acid (FA) molecules are connected on the surface of 5-FU-loaded nanoparticle MIL-101(Fe)-NH<sub>2</sub> by a covalent conjugation. Cytotoxicity tests showed that the synthesized nanoparticles are biocompatible and can significantly inhibit cell proliferation on SMMC-7721 cells compared with MIL-101(Fe)@FU and free 5-FU. The cell metastasis and invasion experiments proved that the nanoparticles had a good anti-metastasis ability to tumor cells. Mechanistically, MIL-101(Fe)@FU@FA induces apoptosis of SMMC-7721 cells and block cell cycle progression in the G2/M phase. Taken together, the drug-loaded nanoparticles MIL-101(Fe)@FU@FA have the effect of targeting and sustained release to achieve the therapeutic effect.

© 2022 The Authors. Published by Elsevier B.V. on behalf of King Saud University. This is an open access article under the CC BY-NC-ND license (<http://creativecommons.org/licenses/by-nc-nd/4.0/>).

## 1. Introduction

Metal-organic framework (MOFs) materials are a kind of organic–inorganic hybrid materials (He et al., 2021). Porous nanosized metal–organic frameworks (MOFs) have been possible candidates as drug-delivery carriers in view of their versatile porous structures, large porosity, biodegradability and large loadings of drugs (Gao et al., 2021; Wu et al., 2017(Wu et al., 2016) Li et al., 2020; Sun et al., 2021; Troyano et al., 2020; Zhang et al., 2020). Some porous nanosized metal–organic frameworks show desirable loading, but unsatisfactory in controlled release with most of a burst effect and localized release

\* Corresponding author.

E-mail address: [liangjyt@163.com](mailto:liangjyt@163.com) (L. Liang).

Peer review under responsibility of King Saud University.



at tumor sites. In order to enlarge the drug loading amount and the controlled release rate, it is necessary to optimize the size and morphology of the porous metal organic frameworks, specific surface should be increased and some modification of the structure introduced. With fascinating properties such as well-defined pores and low toxicity, MIL101-NH<sub>2</sub>(Fe) is one of the most effective drug carrier materials in terms of its very large aperture, high porosity and biodegradability, some nanosized MIL-101-NH<sub>2</sub>(Fe) and its composites are used as drug nanocarriers (Liu et al., 2014; Wyszogrodzka-Gawel et al., 2019). And some multifunctional composite drug-delivery carriers are developed with the function of MR or fluorescence imaging and folic acid, RGD or DNA-functionalized (Gao et al., 2019; Ruan et al., 2020; Shi et al., 2018; Cherkasov et al., 2020; Kahn et al., 2017; Qin et al., 2020; Zhou et al., 2020; Pan et al., 2020). However, further study on those multifunctional drug-delivery systems is limited and the anti-metastasis assay, mechanistic analysis have been not systemically researched.

To reduce toxicity of the anticancer drug to normal cells and enhance antitumor effects, modification of the drug carrier with targeted molecules is a good idea. Folic acid (FA) is a nutrient that is essential to the body and needed by cell division, one-carbon metabolism and nucleotide biosynthesis. Folate receptor (FR) is a glycoprotein expressed at high levels on the surface of tumor cells, such as liver cancer, breast cancer, ovarian cancer, endometrial cancer, but minimally distributed on normal tissues. Folic acid binds to the FR with high affinity and gets internalized via folate receptor-mediated endocytosis role into the cell (Assaraf et al., 2014). A range of exogenous substances such as liposomes, macromolecules and composite nanoparticles can be bound with folic acid via covalent conjugation. (Qu et al., 2020; Benchaala et al., 2014; Stella et al., 2014). The folate composites could still be identified by the folate receptor, and folate-receptor-expressing cells can still selectively aggregate such folate composites. In addition, the folic acid is stable, easily bonded and biocompatible make it an ideal target molecule in drug delivery systems (Yang et al., 2017). So many folate-conjugated nanomaterials have been synthesized and developed in tumor targeting image, drug delivery and chemotherapy (Stella et al., 2007; Zhang et al., 2010; Kumar et al., 2019; Liu et al., 2021).

5-Fluorouracil (5-FU) is a kind of antimetabolic drug that is highly applied in clinical application as anticancer agent for the treatment of various tumors. It is a cycle-specific antitumor agent and its inhibitory effect on the proliferation stage leads to apoptosis of cancer cells. The small molecule character of 5-FU promotes the rapid development and pharmaceutical applications in nano-sized drug delivery system (DDS) (Fang et al., 2021; Matsuda and Sasaki, 2004; Amini-Fazi et al., 2019; Ashwanikumar et al., 2014; He et al., 2021).

Herein, a MOF-based tumor-targeting nanoparticle MIL-101(Fe)@FU@FA was designed and synthesized for targeted delivery of 5-FU to FR-overexpressing cancer cells using ferric chloride and 2-amino-teraphthalic acid. 5-FU is encapsulated into MIL-101(Fe)-NH<sub>2</sub> through a non-covalent interaction, and then the targeting reagent FA is covalently conjugated on the external surface of the nanoparticle through an amide bond. The physicochemical characteristics of the particle size and morphology were investigated. The characteristics of drug release in vitro were investigated by UV spectrophotometer. The biological properties of MIL-101(Fe)@FU@FA nanoparticles were investigated and cell death mechanisms were further carried out through anti-metastasis assay, cell cycle and cell apoptosis analysis.

## 2. Experimental

### 2.1. Material and methods

All of the starting reagents and solvents were of the analytical reagent grade (AR) without further purification. Scanning

electron microscope (SEM) images were acquired using a ZEISS Sigma 300 scanning electron microscope and the accelerating voltage in the process of testing is 0.02–30 kV. Powder X-ray diffractometer (PXRD) was performed with Bruker D8 diffractometer equipped with monochromatized Cu-K $\alpha$  ( $\lambda = 1.5418 \text{ \AA}$ , 40 kV, 40 mA) radiation. Fourier transform infrared spectroscopy was performed using a NICOLET iS50 FT-IR spectrometer with KBr pellets in the range of 4000 to 400 cm<sup>-1</sup>. Zeta potential and particle size were measured by Malvern Zetasizer Nano ZS90 particle size potentiometer (Malvern Instruments Limited, U.K). Thermogravimetric analyses (TGA) of the samples were performed on an STA 449-F5 analyzer under N<sub>2</sub> atmosphere at a heating rate of 10 °C·min<sup>-1</sup> from RT to 800 °C. The UV-Vis spectra were obtained on a Thermo Evolution 220 UV-Visible Spectrophotometer. The specific surface area and pore size distribution of the samples were measured by N<sub>2</sub> adsorption-desorption at 77.3 K using an ASAP 2460 Version 3.00.

### 2.2. Preparation of MIL-101(Fe)@FU@FA

MIL-101(Fe) was synthesized solvothermally according to procedures previously reported with a little modification (Gao et al., 2017). 2-Aminoterephthalic acid (NH<sub>2</sub>-H<sub>2</sub>BDC) (0.0748 g, 0.412 mmol) and FeCl<sub>3</sub>·H<sub>2</sub>O (0.225 g, 0.833 mmol) were dissolved in 5 mL DMF. The mixed solution is ultrasonic and sealed into a Teflon-lined stainless steel autoclave and then heated to 110 °C in an oven for 12 h. After slowly cooled to room temperature, brown powder was obtained after centrifugal separation and washed with DMF (2 × 30 mL) and acetone (3 × 30 mL).

The anticancer drug 5-FU was dissolved in methanol, dried nanoparticles of MIL-101(Fe) were added, and then the mixture was magnetically stirred for 6 h. Then the product was centrifuged (10 000 rpm, 3 × 10 min), washed with DMF (2 × 30 mL) and methanol (3 × 30 mL), and then dried at 60 °C overnight.

Folic acid (50 mg, 0.113 mmol) was dissolved in carbonate buffer (25 mL, 1 mol/L, pH 9.6), then 1-ethyl-3-(3-dimethylammoniumpropyl)carbon-2-imine hydrochloride (EDC) (33 mg, 1.72 mmol) and N-butylhydroxydiimide (NHS) (20 mg, 1.72 mmol) were added under magnetic stirring. The mixture was reacted for 30 min to get a clear pale yellow liquid, and then dried MIL-101(Fe) nanoparticles (20 mg) were added. The reaction was continued for six hours in the dark. At the end of the reaction, the reaction solution was centrifuged and washed 3 times with methanol. The precipitate was dried overnight in vacuum to get a light brown powder.

### 2.3. Establishment of a standard curve

Anticancer drug molecule 5-FU was selected, and the standard curve was established according to its absorption wavelength to determine the maximum wavelength. Different solvents (PBS solution with pH 7.4 and mixed phosphate solution with pH 6.8) of 5-FU were used to prepare 5-FU solution with concentration of 20  $\mu\text{g/mL}$ , respectively. Full wavelength scanning was carried out with UV spectrophotometer, and the detection wavelength was determined.

The establishment of a standard curve: The 5-FU drug molecule (2 mg) was added into the mixed phosphate solution

(pH 7.4), dissolved by ultrasound, moved to a 100 mL volumetric flask and shaken evenly at constant volume to be a reserve solution (20  $\mu\text{g/mL}$ ). Then pipetting gun was used to remove different volumes of the reserve solution, and the corresponding solvent was used to dilute the working solution in a series of concentrations of 2, 4, 6, 8, 10  $\mu\text{g/mL}$ . The absorbance was measured at the wavelength of 265 nm, and the standard curve was made by linear regression between the absorbance and the concentration of working liquid.

#### 2.4. Determination of drug loading of MIL-101 (Fe)@FU nanoparticles

The 5-FU drug molecules carried in nanoparticles of MIL-101 (Fe)@FU@FA (0.1 mg) were released by dissolved the nanoparticles in hydrochloric acid solution (1 mL, 1 mol/L) to destroy the MIL-101(Fe) framework completely. After filtration with a 0.22  $\mu\text{m}$  microporous membrane, methanol was added to the solution and volume-ized into a volume-volume flask (10 mL). The absorbance of the sample was measured by UV–Vis spectrophotometer. Put into the established 5-FU standard curve, and the drug loading was calculated to be  $28.84 \pm 0.002\%$ .

#### 2.5. Assessment of drug release

The drug-loaded nanoparticles were placed in a dialysis bag (MWCO500) on a rotary shaker with different pH PBS solutions (pH 7.4 and 6.8). A certain amount of solution was taken out at regular intervals (buffer solution of the same volume was added in time), and the drug content was tracked and detected by UV–Vis ultraviolet spectrum.

In vitro release experiments of MIL-101(Fe)@FU@FA were carried out in phosphate buffer solution with pH 7.4 and 6.8. MIL-101 (Fe)@FU@FA (5 mL) was precisely removed with a pipette gun, placed in a pre-treated dialysis bag, and put into 200 mL of phosphate buffer solution. Dialysate (2 mL) was taken at the set interval time point, and dialysis buffer medium of the same volume was added to ensure the volume of dialysis fluid constant. After dialysis medium (2 mL) was filtered with 0.45  $\mu\text{m}$  microporous membrane, the drug content at each sampling point was measured and the cumulative release rate was calculated.

#### 2.6. Cell viability assay by CCK-8

The cytotoxicity of the materials was measured by the CCK-8 experiment. When the density of SMMC-7721 liver adenocarcinoma cell line (folate receptor positive tumor cells line) grew to about 70%-80% of confluence, the cells were digested with trypsin and collected by centrifuge and prepared into cell suspension. The cell suspension was placed in a 96-well plate (density was  $5.0 \times 10^3$  cells/well) and cultured. The cell culture medium containing different concentrations of nanocarriers was added to incubate the cells for 24 h. CCK-8 (10  $\mu\text{L}$ /well) reagent was added, and the cells were incubated in an oven at 37  $^{\circ}\text{C}$  for 30 min. The absorbance value (OD value) of each well was measured at 450 nm with the enzyme-linked immunoassay (ELISA), and the cell activity was calculated.

#### 2.7. Invasion and migration capacity

**Invasion** The preconfigured matrix glue was laid flat in the upper chamber of Transwell and placed in a 37 $^{\circ}\text{C}$  incubator for solidification for 1–2 h to make it gelatinous. The full flask of SMMC-7721 cells were digested and the SMMC-7721 cells were re-suspended on free 5-FU, MIL-101(Fe)@FU, MIL-101 (Fe)@FU@FA and serum-free medium, respectively. 100  $\mu\text{L}$  cell suspension was directly inoculated into the upper chamber of Transwell at a density of  $1 \times 10^6$  cells/well, and 500  $\mu\text{L}$  DMEM medium containing 10% FBS was added into the lower chamber. After the cells were incubated in the incubator for 48 h, the Transwell chamber was removed and the unin-vaded cells in the upper chamber were gently wiped with cotton swabs. Fixed with 4% paraformaldehyde for about 15 min, and stained with crystal violet. It was washed with PBS for 3 times and air-dried. The Transwell chamber was placed on slides and photographed under an inverted microscope for quantification.

**Migration** SMMC-7721 cells were resuspended with free 5-FU, MIL-101(Fe)@FU, MIL-101 (Fe)@FU@FA and serum-free medium, respectively. 100  $\mu\text{L}$  cell suspension was directly inoculated into the upper chamber of Transwell at a density of  $1 \times 10^6$  cells/well, and 500  $\mu\text{L}$  DMEM medium containing 10% FBS was added into the lower chamber. The cells were incubated in an incubator for 24 h and removed from the Transwell chamber. The same fixed staining procedure was repeated and the migrating cells were photographed and quantified under an inverted microscope.

#### 2.8. Apoptosis and cell cycle

**Apoptosis** SMMC-7721 cells ( $2.0 \times 10^5$  cells/well) were cultured in 6-well plates. After the cells grew to suitable density, the cell culture medium containing free 5-FU, MIL-101(Fe)@FU, MIL-101 (Fe)@FU@FA was added respectively. Untreated cells in DMEM medium containing 10% fetal bovine serum were used as control group. After 24 h, cell specimens were prepared for cell apoptosis detection. Add 500  $\mu\text{L}$  EDTA-free trypsin to each well of wall cells attached to the 6-well plate, shake well and digest until the wall cells are blown off and centrifuged. Carefully suck out the supernatant and add 1 mL precooled 4  $^{\circ}\text{C}$  PBS buffer for centrifugal washing, repeat twice. The cells were re-suspended in 1 mL binding buffer and stained with Annexin V-FITC/PI apoptosis detection kit. The apoptosis rate was measured by flow cytometry.

**Cell cycle** SMMC-7721 cells were cultured in drug-containing cell medium containing free 5-FU, MIL-101(Fe)@FU, MIL-101(Fe)@FU@FA. DMEM medium containing 10% FBS was used as control group. The cells were digested, cell suspension was prepared and centrifuged for 10 min. Add PBS buffer and rinse twice, absorb supernatant carefully, add 500  $\mu\text{L}$  precooled ethanol with 70% volume fraction, and fix in refrigerator at 4  $^{\circ}\text{C}$  (2 h). Cells were stained according to the cell cycle detection kit purchased from BioSharp. Before staining, the fixator was washed with PBS and the cells were suspended with 500  $\mu\text{L}$  PI/RNase A (RNase A: PI = 1:9). The cell cycle distribution of each administration group was detected by flow cytometry at room temperature.

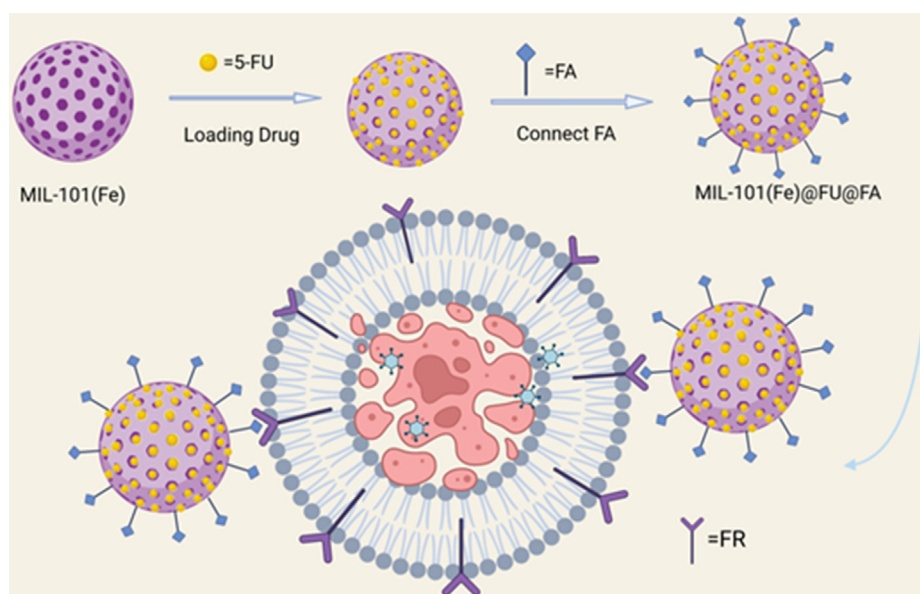
### 3. Results and discussion

#### 3.1. Preparation and characterization of MIL101(Fe)@FU@FA

The preparation process of MIL-101(Fe)@FU@FA is shown in Scheme 1. MIL-101(Fe) was synthesized using 2-aminoterephthalic acid ( $\text{NH}_2\text{-H}_2\text{BDC}$ ) as the ligand and ferric chloride as the metallic ions. The structure of MIL-101(Fe) was confirmed by powder X-ray diffraction (PXRD), FTIR spectra and scanning electron microscopy (SEM) analyses. The PXRD patterns of MIL-101(Fe) match well with the simulated peaks, which demonstrate the successful preparation of MIL-101(Fe) and the phase purity (Fig. 1A). The PXRD patterns of MIL-101(Fe)@FU are basic the same as MIL-101(Fe), indicating the structure of MIL-101(Fe)@FU remain unchanged after incorporation of the drug molecules compared to the parent MIL-101(Fe). The little broaden of the PXRD peaks should be caused by 5-FU drug loading. There are no more peaks and the dominating PXRD peaks of

MIL-101(Fe)@FU are consistent with those of the MIL-101(Fe) spectrum indicating the loaded FU drug molecules inside and outside of the nanoparticles are amorphous phase. Activated folic acid molecules were bonded to the amino group of 2-aminoterephthalic acid on the surface of nanoparticles through conjugation of the non-targeted carboxyl group of folic acid. There are characteristic peaks of folic acid and MIL-101(Fe) in the PXRD patterns of MIL-101(Fe)@FU@FA, indicating the folic acid are successfully conjugated to MIL-101(Fe)@FU. The PXRD patterns of MIL-101(Fe)@FU@FA are weak compared to folic acid, indicating the nanoscale characterization of the materials.

Fourier-transform infrared (FTIR) spectra analyses of MIL-101(Fe), MIL-101(Fe)@FU and MIL-101(Fe)@FU@FA were carried out. FTIR spectra of MIL-101(Fe)@FU@FA further confirmed that FA can be covalently connected on surface of MIL-101(Fe)@FU under gentle conditions. As shown in Fig. 1B, the carbonyl stretching vibration of carboxyl of folic acid ( $1694\text{ cm}^{-1}$ ) disappeared and the N-H stretching vibration of  $-\text{NH}_2$  in MIL-101(Fe)- $\text{NH}_2$



**Scheme 1** The synthetic scheme of MIL101@FU@FA.

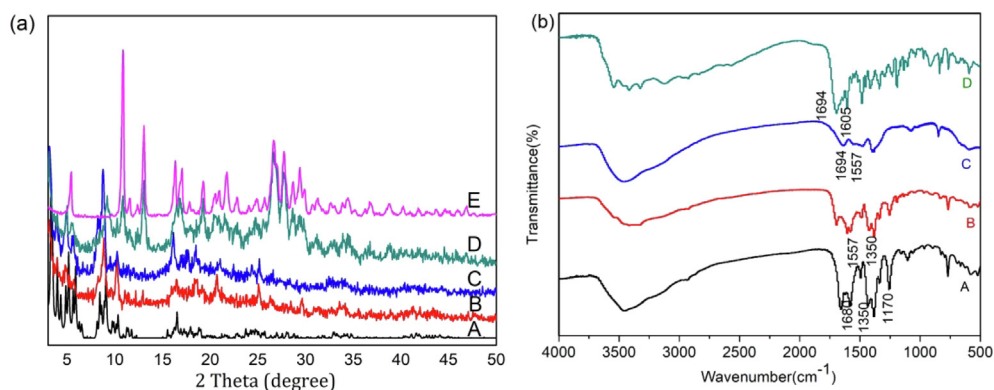


**Fig. 1** (a) Powder X-ray diffraction (PXRD) of (A) simulated, (B) MIL-101(Fe), (C) MIL-101(Fe)@FU, (D) MIL-101(Fe)@FU@FA and (E)FA; (b) FTIR of (A) MIL-101(Fe), (B) MIL-101(Fe)@FU, (C) MIL-101(Fe)@FU@FA and (D) FA.

( $1694\text{ cm}^{-1}$ ) decreased. This proves that carboxyl on the surface of the nanoparticle is successfully transformed to amide bond. The stretching vibration of the carbonyl bond ( $1557\text{ cm}^{-1}$ ) belongs to the  $-\text{CONH}-$  bond, also proves the formation of the amide bond.

Thermogravimetric analyses (TGA) of MIL-101(Fe) and MIL-101(Fe)@FU were carried out under  $\text{N}_2$  atmosphere at a heating rate of  $10\text{ }^\circ\text{C}\cdot\text{min}^{-1}$  (Fig. S1). The weight loss of about 10% at  $100\text{ }^\circ\text{C}$  with a small endothermic peak for MIL-101(Fe) and MIL-101(Fe)@FU should be the loss of solvent molecules inside the channels. The TGA curve of the MIL-101(Fe)@FU is similar to those of the parent MIL-101(Fe), except for the slower decomposition rate and larger residual mass.

In order to characterize the morphology of MIL-101(Fe) and MIL-101(Fe)@FU, the vacuum-dried samples were detected by scanning electron microscopy (SEM). From the SEM analysis (Fig. 2), it can be seen that MIL-101(Fe) is a homogeneous octahedron nanoparticle with an average diameter of about 500 nm. Different from most other nanomaterials, the surface of MIL-101(Fe) is porous and concave. This should be helpful to load drug molecules. The SEM of MIL-101(Fe)@FU seems to be rough and adsorbed when the nanoparticles are drug loaded but basically maintained the particle shape and size.

Simultaneously, the porosity of the samples was approved by  $\text{N}_2$  adsorption–desorption technique to detect the change of pore structure of MIL-101(Fe) and MIL-101(Fe)@FU@FA (Fig. 3). The BET surface area of MIL-101(Fe) was  $1390.3\text{ m}^2/\text{g}$ , while the surface area was decreased to  $492.2\text{ m}^2/\text{g}$  after targeting-modification and drug-loading. The decrease of surface area proved the successful loading of 5-FU and targeting-modification.

5-FU, as a model antitumor drug, was chosen and loaded into MIL-101(Fe)@FU@FA nanoparticles. In order to measure the drug loading capacity of nanoparticles MIL-101(Fe), UV spectrophotometer was used and the results show that 5-FU had an absorption peak at 265 nm. The standard curve is shown in Fig. S2. After destruction of the MIL-101(Fe)@FU nanoparticles with hydrochloric acid, the contained 5-

FU was exposed. The absorbance was 0.378 determined by UV spectrophotometer. After taking the above 5-FU standard curve, the concentration was  $29.994\mu\text{g}/\text{mL}$ , about  $28.84 \pm 0.002\%$  of the drug goes into the formula. The encapsulation rate was  $77.01 \pm 0.1\%$ .

The normal tissue has a neutral pH value in humans, while the microenvironment around tumor tissue is special (Alfarouk et al., 2011). The tissues surrounding tumor have a low pH value of about 6.8. Therefore, the drug-release experiments was performed at  $37^\circ\text{C}$  under different pH conditions (pH 7.4 and 6.8, phosphate buffer solution) to investigate the drug-release behaviors of MIL-101(Fe)@FU@FA carriers. As shown in Fig. S3, at pH 7.4, only about 66% of 5-FU was released from MIL-101(Fe)@FU@FA carriers after 24 h, whereas 77% of 5-FU was released at pH 6.8. It is clear that acidic pH buffers can burst the drug-release behaviors of MIL-101(Fe)@FU@FA nanoparticles. After 48 h in vitro release test of 5-FU in MIL-101(Fe)@FU@FA, the drug release rates were 74.27% and 90.46% at pH 7.4 and 6.8, respectively. The 5-FU drug delivery for MIL-101(Fe)@FU@FA at pH 7.4 and 6.8 in period of 12 h is mainly governed by a diffusion process. In the first 3 h, the drug release degree of MIL-101(Fe)@FU@FA was only about 28%, which proved that the targeted nanoparticles had an effect of sustained release. MIL-101(Fe)@FU@FA have drug sustained release characteristics, indicating that the introduction of targeted groups does not change the drug release characteristics of nanoparticles.

The particle sizes of MIL-101(Fe), MIL-101(Fe)@FU and MIL-101(Fe)@FU@FA were measured using Nano-ZS90 particle size detector. As shown in Fig.S4, the particle sizes of MIL-101(Fe), MIL-101(Fe)@FU and MIL-101(Fe)@FU@FA are 532 nm, 668 nm and 643 nm, respectively. The results of particle sizes are consistent with results of SEM. The modification process of MIL-101(Fe)@FU and MIL-101(Fe)@FU@FA was also measured by particle size potentiometer. The zeta potential was positive before the addition of folic acid and negative after the addition of folic acid. As shown in Fig.S5, the zeta potential of MIL-101(Fe)@FU was  $+23.8\text{ mV}$  when FU drug molecules were carried. The

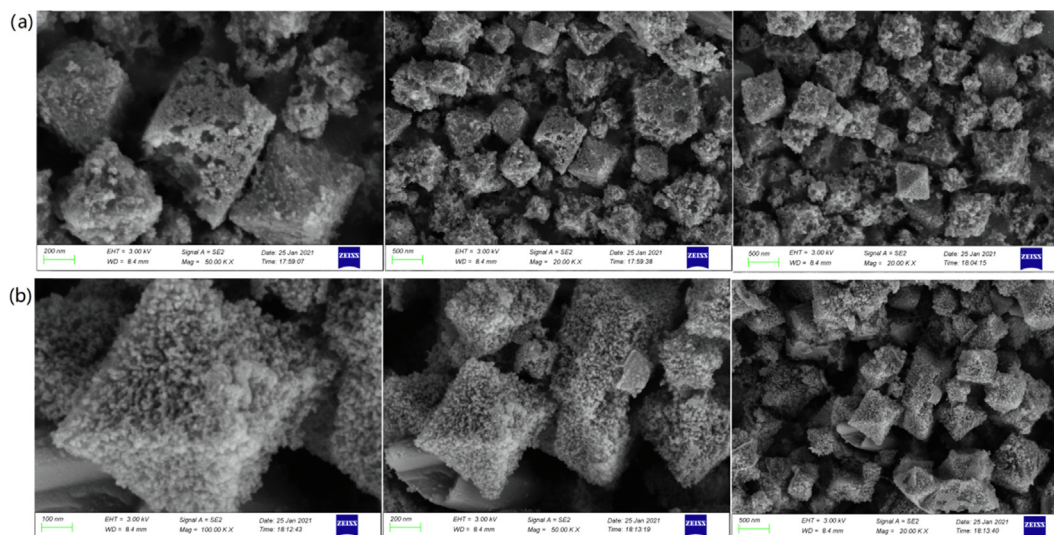
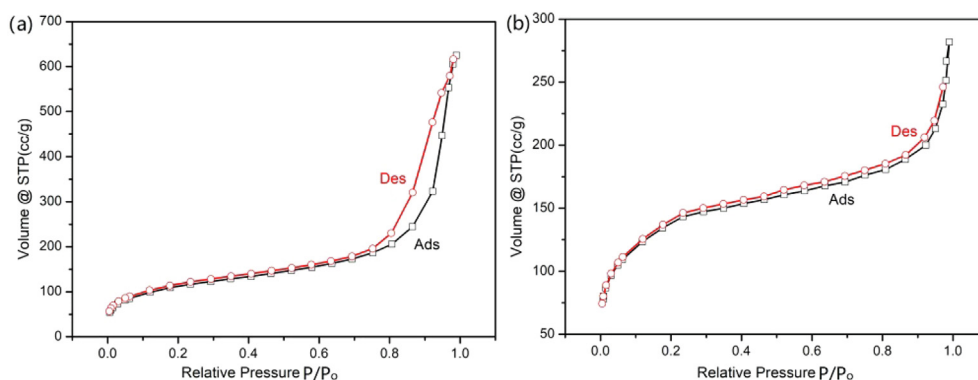


Fig. 2 SEM of synthesized (a) MIL-101(Fe) and (b) MIL-101(Fe)@FU.



**Fig. 3**  $N_2$  adsorption–desorption isotherms of (a) MIL-101(Fe) and (b) MIL-101(Fe)@FU@FA.

zeta potential of MIL-101(Fe)@FU@FA turned to  $-17.7$  mV for the subsequent conjugation of FA (negative charged  $-COOH$ ) (Wu et al., 2016). From this we can extrapolate that the folic acid successfully binds to the MIL-101(Fe)@FU nanoparticles.

### 3.2. Cell viability

The biocompatibility and cytotoxicity of the synthesized materials were evaluated for biological applications. The cell viability of SMMC-7721 hepatocarcinoma cell line incubated with different concentrations (0–200  $\mu\text{g/mL}$ ) of the materials for 24 h was determined by cell counting kit-8 (CCK-8). As can be seen from Fig. 4, the as-prepared MIL-101(Fe) materials had no obvious inhibitory effect on SMMC-7721 cell line at 0–50  $\mu\text{g/mL}$  with a cell viability of more than 90%. When the concentration of MIL-101(Fe) was up to 200  $\mu\text{g/mL}$ , the survival rate of cells was about 73.70%, which indicates that MIL-101(Fe) has no significant effect on the growth of cells and displays good biocompatibility in vitro. As the as-prepared MIL-101(Fe) showed no toxic effects in the range of 0–50  $\mu\text{g/mL}$ , it could be used as a nanoparticle drug carrier. In contrast, MIL-101(Fe)@FU and MIL-101(Fe)@FU@FA both have inhibitory effects on the growth of SMMC-7721 cells with a dose-dependent toxicity similar to the free 5-FU. When the concentration of materials was 64  $\mu\text{g/mL}$ , the cell viability were 13.49% and 11.78%, respectively, indicating that MIL-101(Fe)@FU@FA could effectively load 5-FU to achieve therapeutic effect. The  $IC_{50}$  of MIL-101(Fe)@FU@FA is  $7.40 \pm 0.9$ , which is smaller than  $IC_{50}$  of free 5-FU  $8.47 \pm 0.5$ . These data demonstrate that the MIL-101(Fe)@FU@FA has highly efficient and good therapeutic effect

of tumor cells due to the targeting modification and sustained release of drug molecules.

### 3.3. Invasion and migration

The metastasis course of cancer cells is very complex. There are several continuous and dynamic biological processes. Cell invasion and migration are the main points of metastasis (Chaffer and Weinberg, 2011). Cell invasion is a hallmark of cancer and is characterized by the movement of cells through a three-dimensional matrix, leading to the reshaping of the cellular environment. Studying the ability of cells to migrate and invade in vitro is a useful tool for assessing the aggressiveness of solid cancers, including liver cancer. Many researches revealed that 5-FU can induce cell apoptosis through different mechanisms (Brenes et al., 2007). The anti-metastatic effect of MIL-101(Fe)@FU@FA may be influenced by the nanoparticle size and the targeting-modification. Herein, the anti-metastatic effect of MIL-101(Fe)@FU@FA was performed by cell invasion and migration. The results of invasion and migration are shown in Fig. 5. Invasion assays showed that the free 5-FU, MIL-101(Fe)@FU and MIL-101(Fe)@FU@FA groups showed different degrees of invasion inhibition on SMMC-7721 cells, compared with the control group. It was observed that MIL-101(Fe)@FU@FA nanoparticles significantly inhibit invasion and show the least number of cell invasion. The invasion rates of MIL-101(Fe)@FU and free 5-FU were  $30.48 \pm 1.62\%$  and  $41.90 \pm 1.06\%$ , respectively. The analysis of the corresponding intrusion detection statistical data further confirmed that the invasion rate of MIL-101(Fe)@FU@FA group was the lowest ( $14.28 \pm 0.71\%$ ). It was observed that the MIL-101(Fe)@FU@FA nanoparticles can

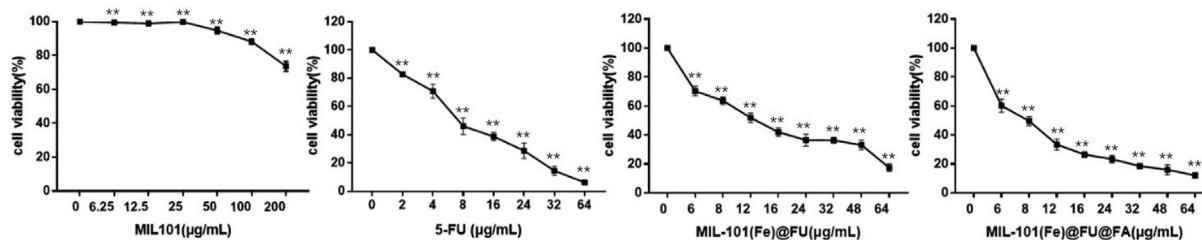


**Fig. 4** Viabilities of SMMC-7721 cells cultured with different concentrations of drugs.

inhibit invasion more effectively than MIL-101(Fe)@FU and the free 5-FU.

The cell migration results were similar with the cell invasion rates (Fig. 5b). The free 5-FU, MIL-101(Fe)@FU and MIL-101(Fe)@FU@FA groups had different degrees of inhibition on the migration of SMMC-7721 cells, compared with the control group. The corresponding intrusion detection statistical data analyses showed that the invasion rates of the free 5-FU, MIL-101(Fe)@FU and MIL-101(Fe)@FU@FA were  $67.81 \pm 1.21\%$ ,  $48.27 \pm 1.43\%$  and  $25.28 \pm 0.11\%$ , respectively. Both the cell migration rates and the cell invasion rates showed that MIL-101(Fe)@FU@FA nanoparticles significantly inhibited migration.

### 3.4. Analysis of apoptosis by DAPI staining

To confirm that the growth inhibitory activity of the synthesized drug-carried materials can really induce apoptosis, changes in different times of apoptosis of SMMC-7721 cells were assayed by Annexin V-FTTC flow cytometry. FR over-expressing SMMC-7721 cancer cells were incubated with different treatment groups for 24 h and apoptosis was analyzed by Annexin V-FTTC flow cytometry. As shown in the

Fig. 6, the percentage of apoptosis in the control group was 3.97%, and the percentage of apoptosis in the free 5-FU, MIL-101(Fe)@FU and MIL-101(Fe)@FU@FA were 6.27%, 14.87% and 28.12%, respectively. The MIL-101(Fe)@FU@FA group showed the highest apoptosis. The results indicated that MIL-101(Fe)@FU@FA nanoparticles could deliver 5-FU to tumor cells more effectively, resulting in apoptotic death of tumor cells. The capability of MIL-101(Fe)@FU@FA to induce SMMC-7721 cells apoptosis was significantly stronger than that of the free 5-FU and MIL-101(Fe)@FU. The cell apoptosis results of MIL-101(Fe)@FU@FA were consistent with the results of invasion and migration, which further proved the targeting role of FA-mediated materials.

### 3.5. Effects of MIL-101(Fe)@FU@FA on the cell cycle

To further study the cell death mechanisms of MIL-101(Fe)@FU@FA, a cell cycle analysis of SMMC-7721 cells incubated in different treatment groups was conducted by flow cytometry. The results in Fig. 7 indicated that the free 5-FU, MIL-101(Fe)@FU and MIL-101(Fe)@FU@FA arrested cell cycle progression to varying degrees in SMMC-7721 cells, compared with

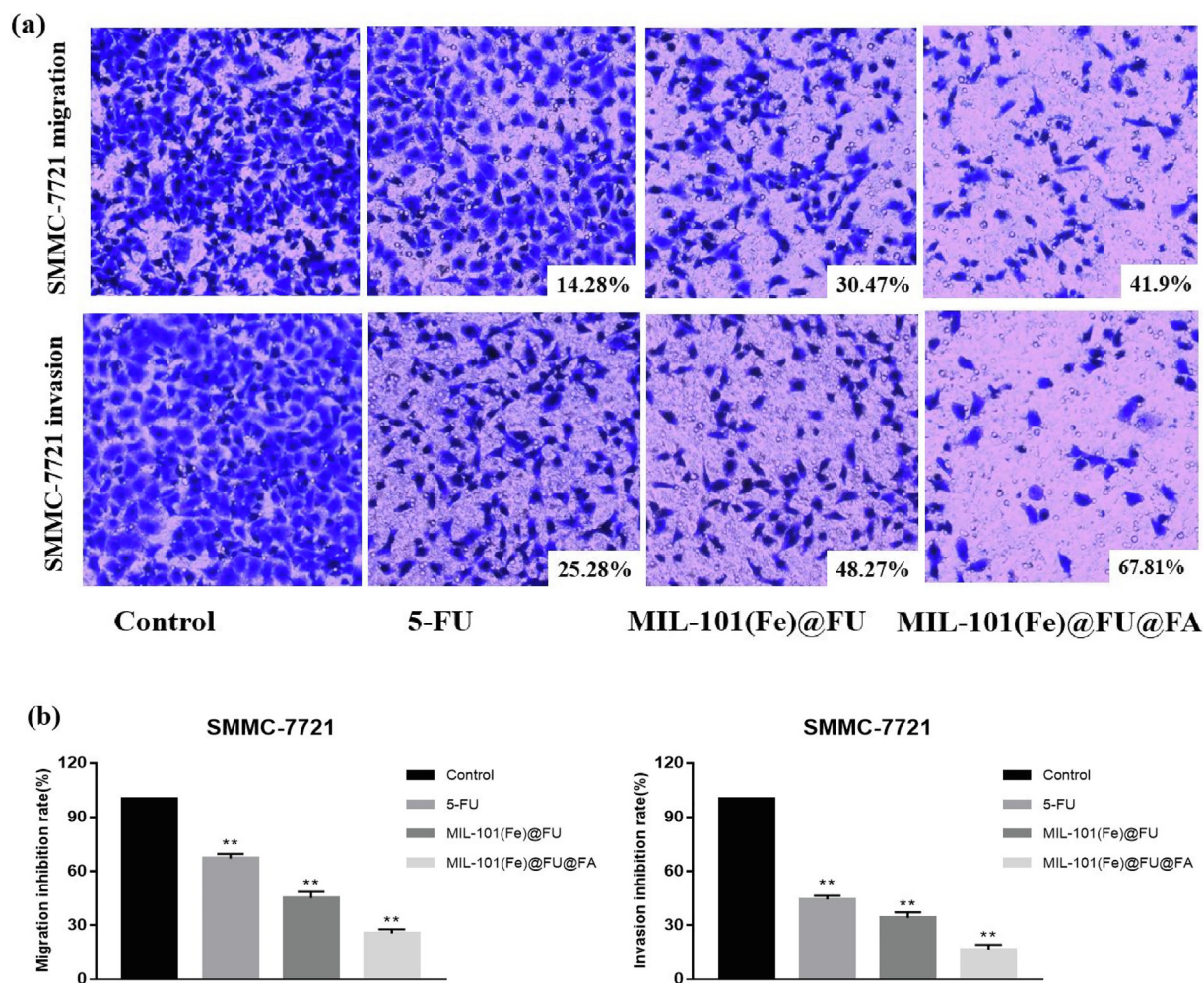


**Fig. 5** Effect of MIL-101(Fe)@FU@FA on the mobility of SMMC-7721 cells. (a) Representative images of invasion and migration, (b) Quantitative analysis of the inhibition of invasion and migration.

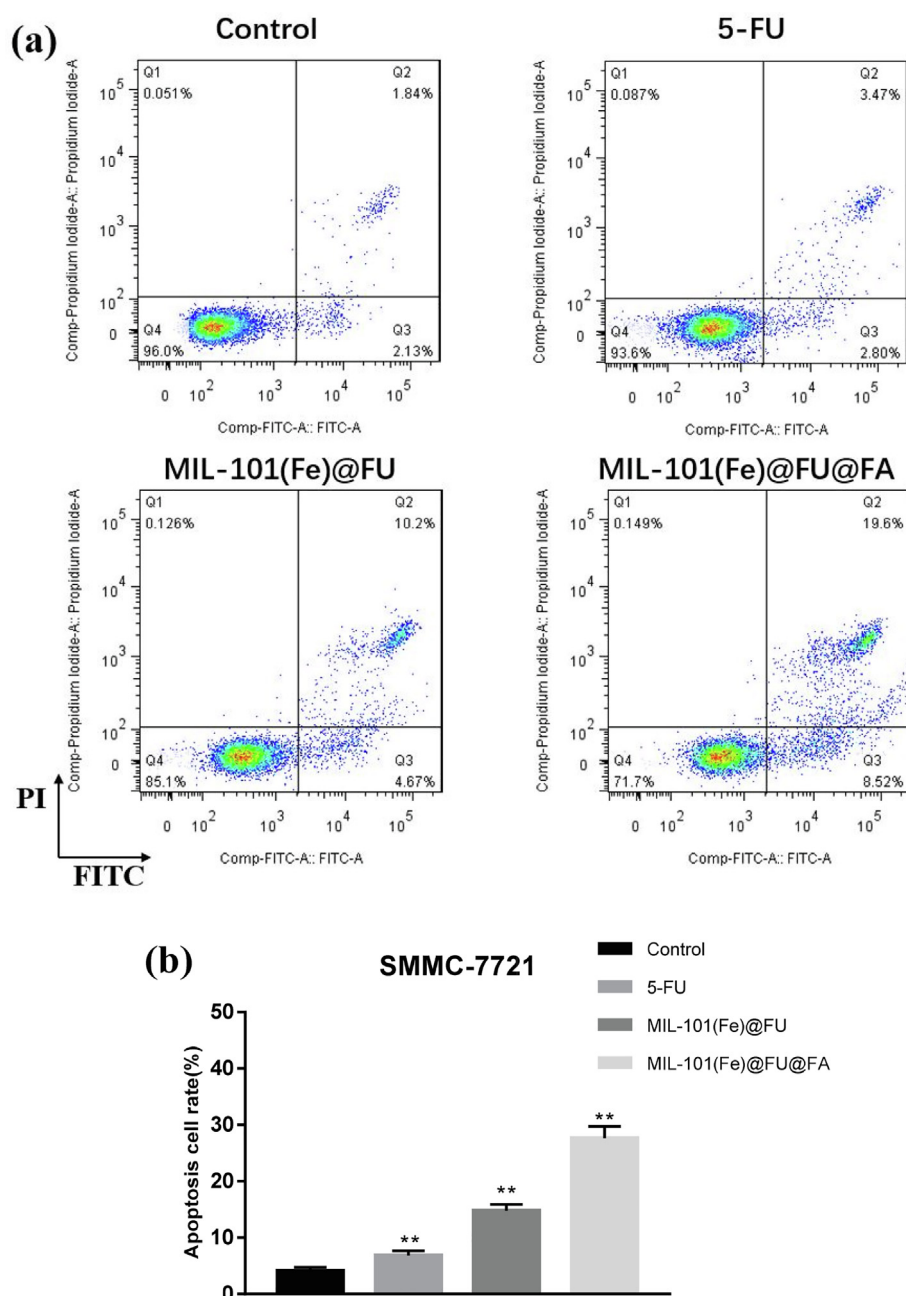


**Fig. 6** Results of apoptosis of SMMC-7721 cells. (a) The image of apoptosis using Annexin V-FITC/PI staining, (b) Statistical analysis results of apoptosis in cells.

the control group. In addition, compared with free 5-FU and MIL-101(Fe)@FU, MIL-101(Fe)@FU@FA could more significantly block cell cycle progression in the G2/M phase of SMMC-7721 cells. It was proved that MIL-101(Fe)@FU@FA could deliver 5-FU to SMMC-7721 cells more effectively, thus blocking the cell cycle progression and inhibiting cell proliferation of SMMC-7721 cells more effectively.

#### 4. Conclusion

In conclusion, a nanosized material MIL-101(Fe)@FU@FA has been successfully developed by conjugating functional FA molecules on the surface to achieve targeting therapeutic effect. CCK-8 experiments

showed that the synthesized nanoparticles were biocompatible and exhibited more significant cell proliferation inhibitory action on SMMC-7721 cells compared with the free 5-FU and MIL-101(Fe)@FU alone. Cell invasion and migration experiments showed that MIL-101(Fe)@FU@FA significantly inhibited the invasion and migration of SMMC-7721 cells at non-cytotoxic concentration, showing a good anti-metastasis ability to tumor cells. Furthermore, flow apoptosis results showed that the synthesized nanoparticle carrier could deliver 5-FU to tumor cells more effectively, resulting in apoptotic death of tumor cells. Cell cycle results showed that MIL-101(Fe)@FU@FA could block the cell cycle progression in the G2/M state and inhibiting cell proliferation of SMMC-7721 cells more effectively. These findings indicated that MIL-101(Fe)@FU@FA, as a nanometer carrier, can efficiently delivery 5-FU to FR over-

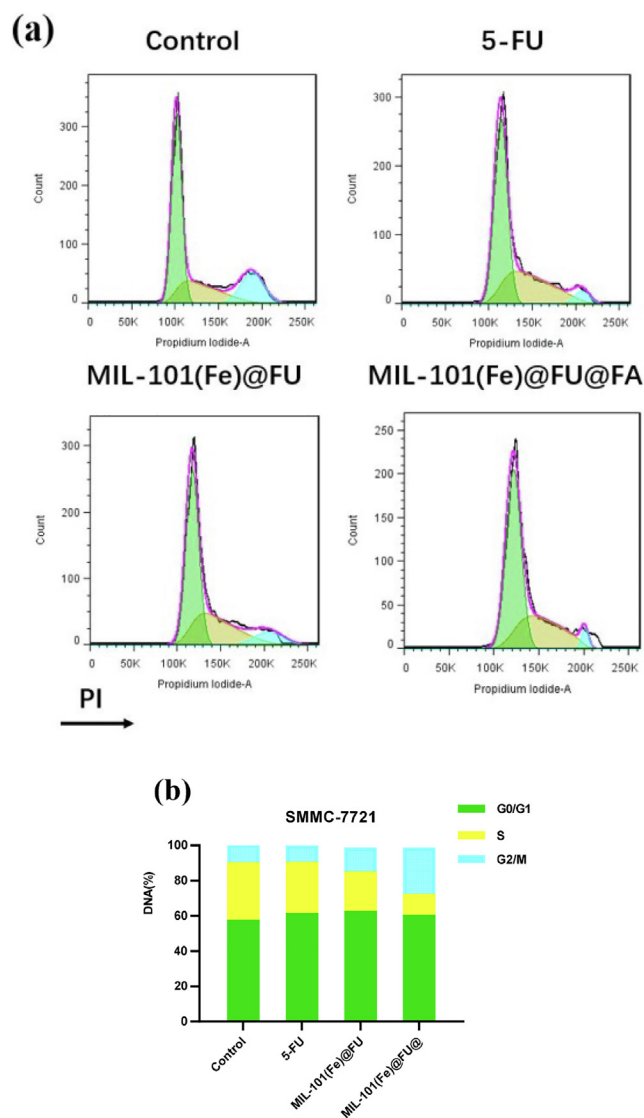


**Fig. 7** (a) Cell cycle analysis of SMMC-7721 cells after treatment with formulation. (b) A bar graph represents the percentage in different phases of cell cycle after treatment with formulation.

expressing cancer cells to improve tumor therapy. The conjugation of targeting molecule into nanometer carrier enhances targeting drug-delivery and has great clinical application potential.

#### Declaration of Competing Interest

The author declare that there is no conflict of interest.

#### Acknowledgements

This work was financially supported by Natural Science of Anhui Province (MB45), 512 Talent Cultivation of Bengbu Medical College (by51201201) and Natural Science Foundation of Bengbu Medical College (2020byzd046).

#### Appendix A. Supplementary material

Supplementary data to this article can be found online at <https://doi.org/10.1016/j.arabjc.2021.103672>.

#### References

- Alfarouk, K.O., Muddathir, A.K., Shayoub, M.E., 2011. Tumor acidity as evolutionary spite. *Cancers* 3 (1), 408–414. <https://doi.org/10.3390/cancers3010408>.
- Amini-Fazl, M.S., Mohammadi, R., Kheiri, K., 2019. 5-Fluorouracil loaded chitosan/polyacrylic acid/Fe<sub>3</sub>O<sub>4</sub> magnetic nanocomposite hydrogel as a potential anticancer drug delivery system. *Int. J. Biol. Macromol.* 132, 506–513. <https://doi.org/10.1016/j.ijbiomac.2019.04.005>.
- Ashwanikumar, N., Kumar, N.A., Nair, S.A., Kumar, G., 2014. Dual drug delivery of 5-fluorouracil (5-FU) and methotrexate (MTX) through random copolymeric nanomicelles of PLGA and polyethylenimine demonstrating enhanced cell uptake and cytotoxicity. *Colloids Surf., B* 122, 520–528. <https://doi.org/10.1016/j.colsurfb.2014.07.024>.
- Assaraf, Y.G., Leamon, C.P., Reddy, J.A., 2014. The folate receptor as a rational therapeutic target for personalized cancer treatment. *Drug Resist. Updates* 17 (4–6), 89–95. <https://doi.org/10.1016/j.drup.2014.10.002>.
- Benchaala, I., Mishra, M.K., Wykes, S.M., Hali, M., Kannan, R.M., Whittum-Hudson, J.A., 2014. Folate-functionalized dendrimers for targeting chlamydia-infected tissues in a mouse model of reactive arthritis. *Int. J. Pharm.* 466 (1–2), 258–265. <https://doi.org/10.1016/j.ijpharm.2014.03.018>.
- Brenes, O., Arce, F., Gätjens-Boniche, O., Diaz, C., 2007. Characterization of cell death events induced by anti-neoplastic drugs cisplatin, paclitaxel and 5-fluorouracil on human hepatoma cell lines: possible mechanisms of cell resistance. *Biomed. Pharmacother.* 61 (6), 347–355. <https://doi.org/10.1016/j.biopha.2007.02.007>.
- Chaffer, C.L., Weinberg, R.A., 2011. A perspective on cancer cell metastasis. *Science* 331 (6024), 1559–1564. <https://doi.org/10.1126/science.1203543>.
- Cherkasov, V.R., Mochalova, E.N., Babenyshev, A.V., Rozenberg, J. M., Sokolov, I.L., Nikitin, M., 2020. Antibody-directed metal-organic framework nanoparticles for targeted drug delivery. *Acta Biomater.* 103, 223–236. <https://doi.org/10.1016/j.actbio.2019.12.012>.
- Fang, Q., Xu, X., Yang, L., Xue, Y., Cheng, X., Wang, X., Tang, R., 2021. Self-assembled 5-fluorouracil-cinnamaldehyde nanodrugs for greatly improved chemotherapy in vivo. *J. Biomater. Appl.* 885328221989539. <https://doi.org/10.1177/0885328221989539>.
- Gao, P., Chen, Y., Pan, W., Li, N., Liu, Z., Tang, B., 2021. Antitumor agents based on metal-organic frameworks. *Angew. Chem.* 60 (31), 16763–16776. <https://doi.org/10.1002/anie.202102574>.
- Gao, X., Cui, R., Song, L., Liu, Z., 2019. Hollow structural metal-organic frameworks exhibit high drug loading capacity, targeted delivery and magnetic resonance/optical multimodal imaging. *Dalton Trans.* 48 (46), 17291–17297. <https://doi.org/10.1039/c9dt03287>.
- Gao, X., Zhai, M., Guan, W., Liu, J., Liu, Z., Damin, A., 2017. Controllable synthesis of a smart multifunctional nanoscale metal-organic framework for magnetic resonance/optical imaging and targeted drug delivery. *ACS Appl. Mater. Interfaces* 9 (4), 3455–3462. <https://doi.org/10.1021/acsami.6b14795>.
- He, S., Wu, L., Li, X., Sun, H., Xiong, T., Liu, J., Huang, C., Xu, H., Sun, H., Chen, W., Gref, R., Zhang, J., 2021. metal-organic

- frameworks for advanced drug delivery. *Acta pharmaceutica Sinica. B* 11 (8), 2362–2395. <https://doi.org/10.1016/j.apsb.2021.03.019>.
- Kahn, J.S., Freage, L., Enkin, N., Garcia, M.A., Willner, I., 2017. Stimuli-responsive DNA-functionalized metal-organic frameworks (MOFs). *Adv. Mater.* 29 (6), 1602782. <https://doi.org/10.1002/adma.20160278>.
- Kumar, P., Huo, P., Liu, B., 2019. Formulation strategies for folate-targeted liposomes and their biomedical applications. *Pharmaceutics*. 11 (8), 381. <https://doi.org/10.3390/pharmaceutics11080381>.
- Liu, W., Yan, Q., Xia, C., Wang, X., Kumar, A., Wang, Y., Liu, Y., Pan, Y., Liu, J., 2021. Recent advances in cell membrane coated metal-organic frameworks (MOFs) for tumor therapy. *J. Mater. Chem. B* 9 (22), 4459–4474. <https://doi.org/10.1039/d1tb00453k>.
- Li, L., Han, S., Yang, C., Liu, L., Zhao, S., Wang, X., Liu, B., Pan, H., Liu, Y., 2020. Glycyrrhetic acid modified MOFs for the treatment of liver cancer. *Nanotechnology*. 31, (32). <https://doi.org/10.1088/1361-6528/ab8c03> 325602.
- Liu, S., Zhai, L., Li, C., Li, Y., Guo, X., Zhao, Y., Wu, C., 2014. Exploring and exploiting dynamic noncovalent chemistry for effective surface modification of nanoscale metal-organic frameworks. *ACS Appl. Mater. Interfaces* 6 (8), 5404–5412. <https://doi.org/10.1021/am500192b>.
- Matsuda, A., Sasaki, T., 2004. Antitumor activity of sugar-modified cytosine nucleosides. *Can. Sci.* 95 (2), 105–111. <https://doi.org/10.1111/j.1349-7006.2004.tb03189.x>.
- Pan, Y., Luo, Z., Wang, X., Chen, Q., Chen, J., Guan, Y., Liu, D., Xu, H., Liu, J., 2020. A versatile and multifunctional metal-organic framework nanocomposite toward chemo-photodynamic therapy. *Dalton Trans.* 49 (16), 5291–5301. <https://doi.org/10.1039/c9dt04804a>.
- Qu, Y., Hao, C., Zhai, R., Yao, W., 2020. Folate and macrophage folate receptor- $\beta$  in idiopathic pulmonary fibrosis disease: the potential therapeutic target? *Biomed. Pharmacother.* 131. <https://doi.org/10.1016/j.biopha.2020.110711> 110711.
- Qin, J.H., Zhang, H., Sun, P., Huang, Y.D., Shen, Q., Yang, X.G., Ma, L.F., 2020. Ionic liquid induced highly dense assembly of porphyrin in MOF nanosheets for photodynamic therapy. *Dalton Trans.* 49 (48), 17772–17778. <https://doi.org/10.1039/d0dt03031g>.
- Ruan, B., Liu, H.L., Xie, L., Ding, H., Zhang, Y., Wu, J., Huang, Z., Shi, D., Jiang, T., Tsai, F.C., 2020. The fluorescence property of zirconium-based MOFs adsorbed sulforhodamine B. *J. Fluorescence*. 30 (3), 427–435. <https://doi.org/10.1007/s10895-020-02531-0>.
- Sun, Y., Jiang, X., Liu, Y., Liu, D., Chen, C., Lu, C., Zhuang, S., Kumar, A., Liu, J., 2021. Recent advances in Cu(II)/Cu(I)-MOFs based nano-platforms for developing new nano-medicines. *J. Inorg. Biochem.* 225. <https://doi.org/10.1016/j.jinorgbio.2021.111599> 111599.
- Shi, Z., Chen, X., Zhang, L., Ding, S., Wang, X., Lei, Q., Fang, W., 2018. FA-PEG decorated MOF nanoparticles as a targeted drug delivery system for controlled release of an autophagy inhibitor. *Biomater. Sci.* 6 (10), 2582–2590. <https://doi.org/10.1039/c8bm00625c>.
- Stella, B., Marsaud, V., Arpicco, S., Géraud, G., Cattel, L., Couvreur, P., Renoir, J.M., 2007. Biological characterization of folic acid-conjugated poly( $H_2N$ PEGCA-co-HDCA) nanoparticles in cellular models. *J. Drug Target.* 15 (2), 146–153. <https://doi.org/10.1080/10611860600935826>.
- Troyano, J., Çamur, C., Garzón-Tovar, L., Carné-Sánchez, A., Imaz, I., Maspocho, D., 2020. Spray-drying synthesis of MOFs, COFs, and related composites. *Acc. Chem. Res.* 53 (6), 1206–1217. <https://doi.org/10.1021/acs.accounts.0c00133>.
- Wu, H., Wang, H., Liao, H., Lv, Y., Song, X., Ma, X., Tan, M., 2016. Multifunctional nanostructures for tumor-targeted molecular imaging and photodynamic therapy. *Adv. Healthcare Mater.* 5 (3), 311–318. <https://doi.org/10.1002/adhm.201500668>.
- Wu, M.X., Yang, Y.W., 2017. Metal-Organic framework (MOF)-based drug/cargo delivery and cancer therapy. *Adv. Mater.* 29 (23), 1606134. <https://doi.org/10.1002/adma.201606134>.
- Wyszogrodzka-Gaweł, G., Dorożyński, P., Giovagnoli, S., Strzempek, W., Pesta, E., Węglarz, W.P., Gil, B., Menaszek, E., Kulinowski, P., 2019. An inhalable theranostic system for local tuberculosis treatment containing an isoniazid loaded metal organic framework Fe-MIL-101-NH<sub>2</sub>-from raw MOF to drug delivery system. *Pharmaceutics*. 11 (12), 687. <https://doi.org/10.3390/pharmaceutics11120687>.
- Yang, X., Wang, Y., Shen, X., Su, C., Yang, J., Piao, M., Jia, F., Gao, G., Zhang, L., Lin, Q., 2017. One-step synthesis of photoluminescent carbon dots with excitation-independent emission for selective bioimaging and gene delivery. *J. Colloid Interface Sci.* 492, 1–7. <https://doi.org/10.1016/j.jcis.2016.12.057>.
- Zhang, J., Deng, D., Qian, Z., Liu, F., Chen, X., An, L., Gu, Y., 2010. The targeting behavior of folate-nanohydrogel evaluated by near infrared imaging system in tumor-bearing mouse model. *Pharm. Res.* 27 (1), 46–55. <https://doi.org/10.1007/s11095-009-0005-1>.
- Zhang, S., Pei, X., Gao, H., Chen, S., Wang, J., 2020. Metal-organic framework-based nanomaterials for biomedical applications. *Chin. Chem. Lett.* 31 (5), 1060–1070. <https://doi.org/10.1016/j.ccl.2019.11.036>.
- Zhou, Z., Li, B., Shen, C., Wu, D., Fan, H., Zhao, J., Li, H., Zeng, Z., Luo, Z., Ma, L., Tan, C., 2020. Metallic 1T phase enabling MoS<sub>2</sub> nanodots as an efficient agent for photoacoustic imaging guided photothermal therapy in the near-infrared-II window. *Small*. 16 (43), 2004173. <https://doi.org/10.1002/sml.202004173>.